

Automated Segmentation of Infected Regions in Chest CT Images of COVID-19 Patients using Supervised Naïve Gaussian Bayes Classifier

Dr. Iyad Muhammad Hatem*

(Received 28 / 6 / 2020. Accepted 20 / 9 / 2020)

□ ABSTRACT □

In this paper, one hundred chest Computed Tomography images of COVID-19 patients were used to build and test Naïve Gaussian Bayes classifier for discriminating normal from abnormal tissues. Infected areas in these images were manually segmented by an expert radiologist. Pixel grey value, local entropy and Histograms of Oriented Gradients HOG were extracted as features for tissue image classification. Based on five-folds classification experiments, the accuracy score of the classifier in this fold reached around 79.94%. Classification was more precise (85%) in recognizing normal tissue than abnormal tissue (63%). The effectiveness in identifying positive labels was also more evident with normal tissue than the abnormal one.

Keywords: Medical image analysis, Image segmentation, COVID-19, CT imaging, Naïve Bayes classifier.

*Associate Professor- Faculty of Mechanical and Electrical Engineering - Tishreen University- Lattakia- Syria.

التقطيع المؤتمت للمناطق المصابة في صور طبقي محوري للصدر لمرضى الكورونا COVID-19 باستخدام مصنف بايز الغاوسي المراقب

د. إياد محمد حاتم*

(تاريخ الإيداع 28 / 6 / 2020. قُبِل للنشر في 20 / 9 / 2020)

□ ملخّص □

استخدمت في هذه الورقة مائة صورة من تصوير مقطعي محوسب للصدر لمرضى الكورونا COVID-19 لبناء واختبار مصنّف Naïve Gaussian Bayes لتمييز النسيج الطبيعية من النسيج غير الطبيعية. قُسمت المناطق المصابة في هذه الصور يدويًا بواسطة أخصائي أشعة خبير. أُجريت عملية استخراج قيمة البكسل الرمادية والانتروبيا المحلية وقيم الهستوغرام للتدرجات الموجهة HOG كميزات لتصنيف صور الأنسجة. استنادًا إلى تجارب تصنيف ذات خمس طبقات، وصلت درجة دقة المصنّف إلى حوالي 79.94%. كان التصنيف أكثر دقة (85%) في التعرف على الأنسجة الطبيعية من الأنسجة غير الطبيعية (63%). كانت أيضاً الفعالية في تحديد المناطق أكثر وضوحًا في الأنسجة الطبيعية من الأنسجة غير الطبيعية.

الكلمات المفتاحية: تحليل الصور الطبية، تجزئة الصورة، كورونا COVID-19، التصوير المقطعي، مصنف Naïve Gaussian Bayes.

*أستاذ مساعد - كلية الهندسة الميكانيكية والكهربائية - جامعة تشرين - اللاذقية - سورية.

Introduction:

As of today, September 20th, 2020, the COVID-19 CORONAVIRUS epidemic had spread to **213 countries and territories** around the world and 2 international conveyances. More than thirty million individuals have contracted the virus worldwide with 964,065 reported deaths [1]. Currently, the adopted microbiological tests for confirming COVID-19 (such as PT-PCR) are not always reachable at emergency sites and their results are not immediately available [2]. The Chest Computed Tomography (CT) proved to have a high sensitivity for diagnosis of COVID-19 and may be considered as a primary tool for the current COVID-19 detection in epidemic areas [3]. Quick identification and early diagnosis of new cases is mainly based on the radiologist work. This will benefit not only the patients but also the response and public health surveillance systems.

The typical findings from chest CT images of patients are bilateral multiple lobular and sub-segmental areas of consolidation and ground-glass opacity [4, 5, 6].

Based on [7] the COVID-19 pneumonia tends to demonstrate on lung CT scans through bilateral, sub-pleural, ground-glass opacities with air bronchograms, ill-defined margins, and a slight predominance in the right lower lobe. Abnormal lung CT findings can be present even in asymptomatic patients, and lesions can rapidly evolve into a diffuse ground-glass opacity predominance or consolidation pattern within 1–3 weeks after onset of symptoms, peaking at around 2 weeks after onset. Old age, male sex, underlying comorbidities and progressive radiographic deterioration on follow-up CT might be risk factors for poor prognosis in patients with COVID-19 pneumonia.

Medical images can sometimes be challenging to read which lay an excessive burden on radiologists. For this reason, many researches has been worked to develop computer-aided diagnosis (CAD) tools to assist evaluation processes. The objective of the work presented in this paper is to automatically distinguish normal from abnormal tissue in axial CT-images of confirmed COVID-19 cases. The manual segmentation of these images was done by a trained radiologist. Three main abnormal areas were labeled: ground class opacification, consolidations and pleural effusions [8].

1 Image Data Set

Three data sets were utilized in this work: the original CT images, the lung mask images and the abnormal mask images.

The original CT Images were downloaded from Italian Society of Medical and Interventional Radiology. These images were cropped and resized after converted from DICM to JPG format. They were then reversely intensity-normalized by taking RGB-values from the JPG-images from areas of air and fat and used to establish the unified Hounsfield Unit-scale (the air was normalized to -1000, fat to -100).

The lung mask images were implemented by using automated lung segmentation model [9]. On the other hand, a manual segmentation of the abnormal areas was performed by using MedSeg online software¹ by an expert radiologist. Figure 1 shows the original, lung mask and abnormal mask images of a selected sample of the database.

¹ <http://htmlsegmentation.s3.eu-north-1.amazonaws.com/index.html>

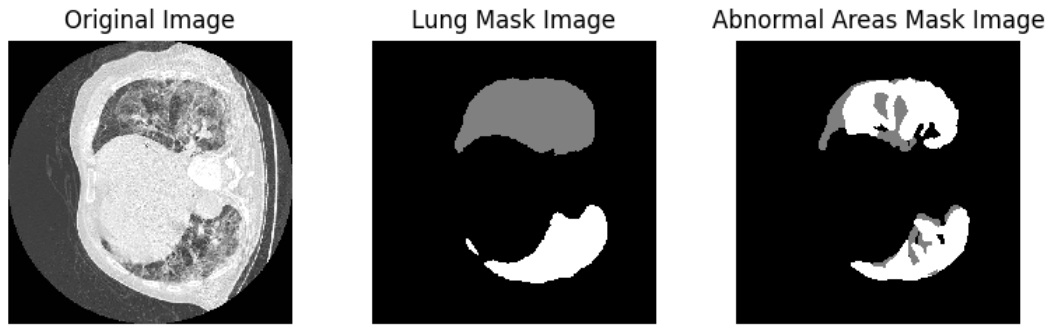


Figure 1: Sample Original Image with its masks

2 Proposed Method

Figure 2 shows the main stages of the proposed methodology in this paper. The image database contains original CT images, mask images of segmented lung areas, and labeled mask images for abnormal and normal tissues.

2.1 Image preprocessing

CT images is susceptible to noise as most of medical images. Different filters have been investigated to reduce noise in CT images.

In the preprocessing stage, two main steps are essential: noise removal and contrast enhancement. For this stage, the median filter followed by anisotropic diffusion filter were applied on all images. These two filters are known for their ability to reduce noise and enhance contrast in medical images in general and in CT images in particular [10, 11, and 12].

2.2 Feature Extraction

Three features were used to build the segmentation classifier. The first feature was the original grey level values in the range [0-255]. The other two features were the local entropy and Histograms of Oriented Gradients (HOG).

2.2.1 Local Entropy

Local entropy as a texture feature has been proved to be robust to irradiation distortion, geometric distortion and noise interference [13, 14]. It is also known for its role as a representative feature of the underlying local data structure in images.

The local entropy in a neighborhood of an image pixel represents the statistical characteristics of that region. In particular, it reflects the variance and heterogeneity within the neighborhood. It is computed by the following equation

$$E(i) = - \sum_{g=1}^N P(g) \log_2 P(g) \quad (1)$$

where:

$E(i)$: image entropy on i^{th} pixel

$P(g)$: the probability of grey level g in the neighborhood of pixel i

N : the image grey level

In a pixel of neighborhood with uniform distribution of grey levels, the local entropy is large. Where, it is small with non-uniform grey scale distribution [15].

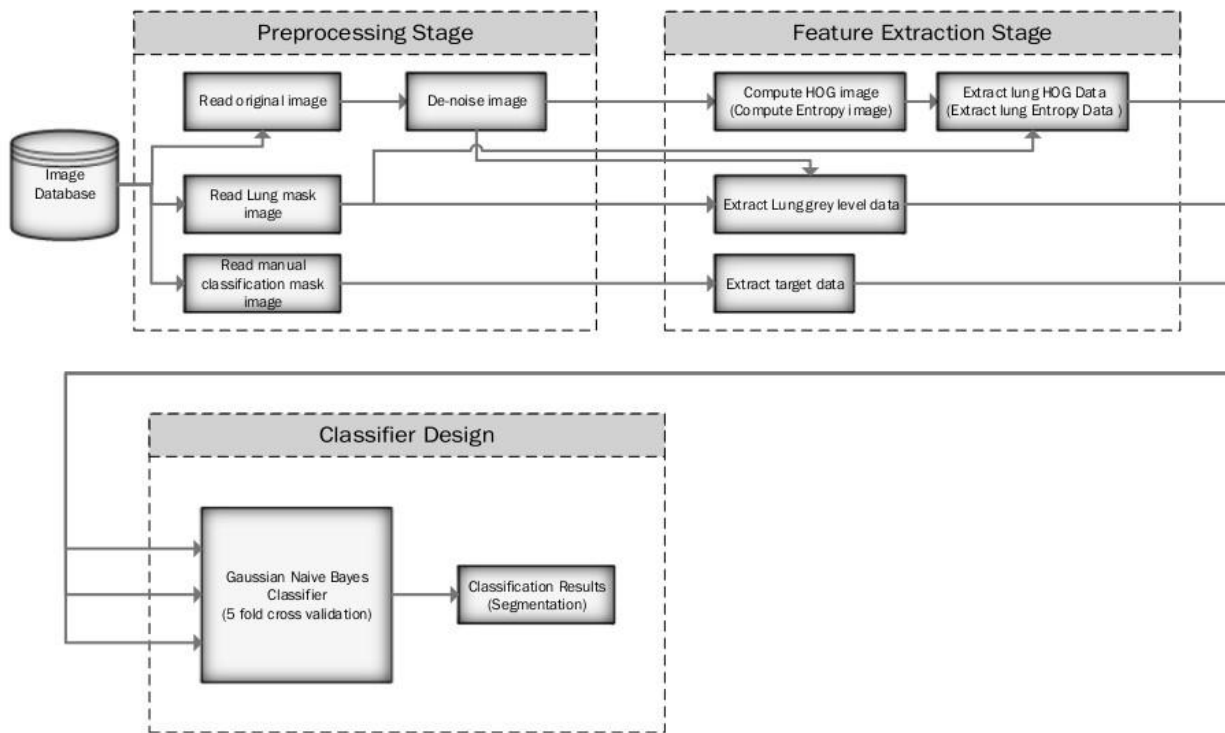


Figure 2 General flow diagram of the proposed method.

2.2.2 Histograms of Oriented Gradients (HOG)

HOG algorithm was firstly introduced by Dalal [16]. HOG descriptors are widely used in computer vision applications and image processing for object detection and segmentation [17, 18]. HOG seeks to extract features resemble appearance and shape of objects based on the calculation of distribution of local gradients. It is proved good ability to define a strong texture and shape. The following steps outlines the procedure of HOG

1. First, Image is divided into cells
2. Then, gradients are calculated in each cell
3. According to determined gradient values, histograms are constructed
4. Finally, histograms are normalized.

2.3 NAIVE BAYES CLASSIFIER

Naive Bayes Classifier belongs to a family of probability classifiers. Despite its simplicity compared to other sophisticated classifiers, it has the advantage of speed performance in training and prediction on high-dimensional data sets. It also requires only small size of data for referring the relevant parameters. Furthermore, classification results of this method are easily interpreted contrary to other classifiers such as neural networks [22].

According to Bayes' theorem, the conditional probability that an event x belongs to a class k can be calculated from the conditional probabilities of finding particular events in each class and the unconditional probability of the event in each class. That is, for given data, $x \in X$, and C classes, where X denotes a random variable, the conditional probability that an event x belongs to a class k can be calculated by using the following equation:

$$P(c_k|x) = P(c_k) \frac{P(x|c_k)}{P(x)} \quad (2)$$

Equation (2) shows that the calculation of $(P(c_k|x))$ is a pattern classification problem since it finds the probability that the given data x belongs to class k and we can decide the optimum class by choosing the class with the highest probability among all possible classes, C , which can minimize the classification error. For doing so, we need to estimate $(P(x|c_k))$ and assume that any particular value of vector x conditional on c_k is statistically independent of each dimension and can be written as follows:

$$P(x|c_k) = \prod_{i=0}^n P(x_i|c_k) \tag{3}$$

where x is a n -dimensional vector data $x = (x_1, x_2, \dots, x_n)$.

In our particular case of Naive Gaussian Bayes classification the likelihood (or generative model) of the class (c_k) is expected to be normally distributed:

$$P(x_i|c_k) = \frac{1}{\sqrt{2\pi}\sigma_{c_k}} e^{-\frac{(x_i - \mu_{c_k})^2}{2\sigma_{c_k}^2}} \tag{4}$$

with the mean μ_{c_k} and the standard deviation σ_{c_k} of the associated class c_k . Therefore, each training cycle of the classifier adjusts/calculates the relevant parameters $(\mu_{c_k}, \sigma_{c_k})$ for the corresponding features (x_i) and respective classes. The estimated class value of an acquired data x is assigned (predicted) by using its probability of being of class k and the method of Maximum A Posteriori (MAP) estimation:

$$Class(x) = \underset{k}{\operatorname{argmax}} P(c_k) \prod_{i=1}^n P(x_i|c_k) \tag{5}$$

where the denominator $(P(x))$ is omitted since the value is the same for all classes.

Table 1: Confusion Matrix of Classification

	Classified as Normal	Classified as Abnormal
normal	True Positive [tp]	False Negative [fn]
abnormal	False Positive [fp]	True Positive [tn]

2.4 Performance measures for classification

The correctness of a classification can be evaluated based on the elements of what is known as the confusion matrix (shown in table 1). This matrix includes four parameters:

1. the number of correctly recognized class examples (true positives),
2. the number of correctly recognized examples that do not belong to the class (true negatives),
3. and examples that either were incorrectly assigned to the class (false positives)
4. or that were not recognized as class examples (false negatives).

In binary classification the most often used measures based on the elements of the confusion matrix are [23]:

Accuracy: This metric evaluates the overall effectiveness of a classifier

$$Accuracy = \frac{tp + tn}{tp + fn + fp + tn} \tag{6}$$

Precision: It reflects class agreement of the data labels with the positive labels given by the classifier

$$Precision = \frac{tp}{tp + fp} \quad (7)$$

Recall (Sensitivity): It measures effectiveness of a classifier to identify positive labels

$$Recall = \frac{tp}{tp + fn} \quad (8)$$

F1Score: This metric investigates relations between data's positive labels and those given by a classifier. It also represents the harmonic mean of precision and recall

$$F1Score = \frac{2 \cdot tp}{2 \cdot tp + fn + fp} \quad (9)$$

Specificity: It measures of how effectively a classifier identifies negative labels

$$Specificity = \frac{tn}{fp + tn} \quad (10)$$

AUC (Area under the curve): It is a measure of Classifier's ability to avoid false classification

$$AUC = \frac{1}{2} \left(\frac{tp}{tp + fn} + \frac{tn}{fp + tn} \right) \quad (11)$$

Table 2: The results of averaging the five folds experiments

	Classified as Normal	Classified as Abnormal			
Normal	919,915	121,067			
Abnormal	160,763	203,225			
Recall	Precision	F1score	Accuracy	Specificity	AUC
0.8837	0.8512	0.8672	0.7994	0.5583	0.7210

3 Experimental results

We developed the proposed method using Python language and OpenCV 3.2.0 and JetBrains PyCharm 2020, and run it on Ubuntu 18.04.4 LTS computer with Intel® Core™ i5-2450M CPU @ 2.50GHz × 4 and 4.0 GB RAM.

The objective of this work was to investigate the ability of using simple classifier to distinguish infected tissue in CT lung images of COVID-19 patients. At the beginning, classification data were collected from all sample images. As a result, three feature vectors of the lung area pixels were created from 100 masked images. These three vectors represented: original grey value, local entropy, and histogram of oriented gradient (HOG). Meantime, target vector was also constructed for these feature vectors that possessed two values (1 and 0) corresponded to normal and abnormal tissues.

Five-fold stratified cross-validation approach was used to test the classifier. For this, the complete data set was divided into five partitions. This partitioning took in account the ratio of class data sizes. At every fold, four partitions (training set) out of these partitions were used for classifier buildup. The remaining partition was used for classifier evaluation as a test set. The training/testing procedure was repeated five times with different data partitions.

Table 2 shows the results of one fold of the experiment. It presents the confusion matrix with the classification metrics. The accuracy score of the classifier in this fold reached around 79.94%. Classification was more precise (85%) in recognizing normal tissue than abnormal tissue (63%). The effectiveness in identifying positive labels was also more evident with normal tissue than the abnormal one. Finally the F1-score confirms the above results and shows high relation (87%) between predicted normal tissue labels and data labels.

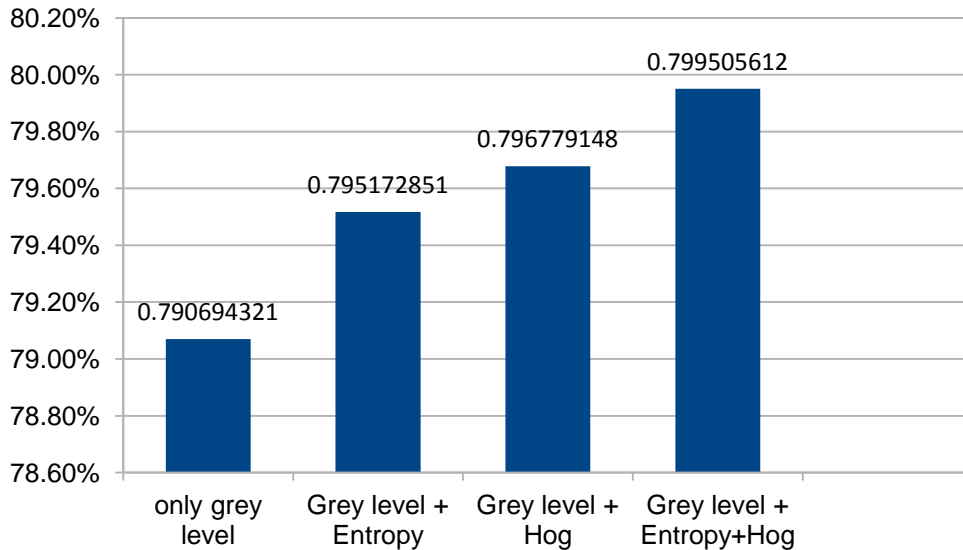


Figure 2: Results of Classification with five-folds experiments

To show the significance of extracted features, the classification method was investigated with four different setups. First, only the grey value was used to build the classifier. Then the two features (entropy and HOG) were added separately to the grey value. Last, the three features were used. Figure 3 shows the results of averaging the five folds experiments for every classifier. The enhancement in classification rate is obvious when adding the entropy and HOG features to the grey level. Nonetheless, this increase contributes to nearly one percent of the classification rate.

Finally, Figure 4 shows the segmentation results on two samples of the tested images. On the left, we show the manual segmentation of these two images and on the right we present the output of segmentation by our proposed method. Apparently, the classifier missed few regions of infected lung. However, the classifier was able to recognize abnormal tissues in all tested samples to some extent.

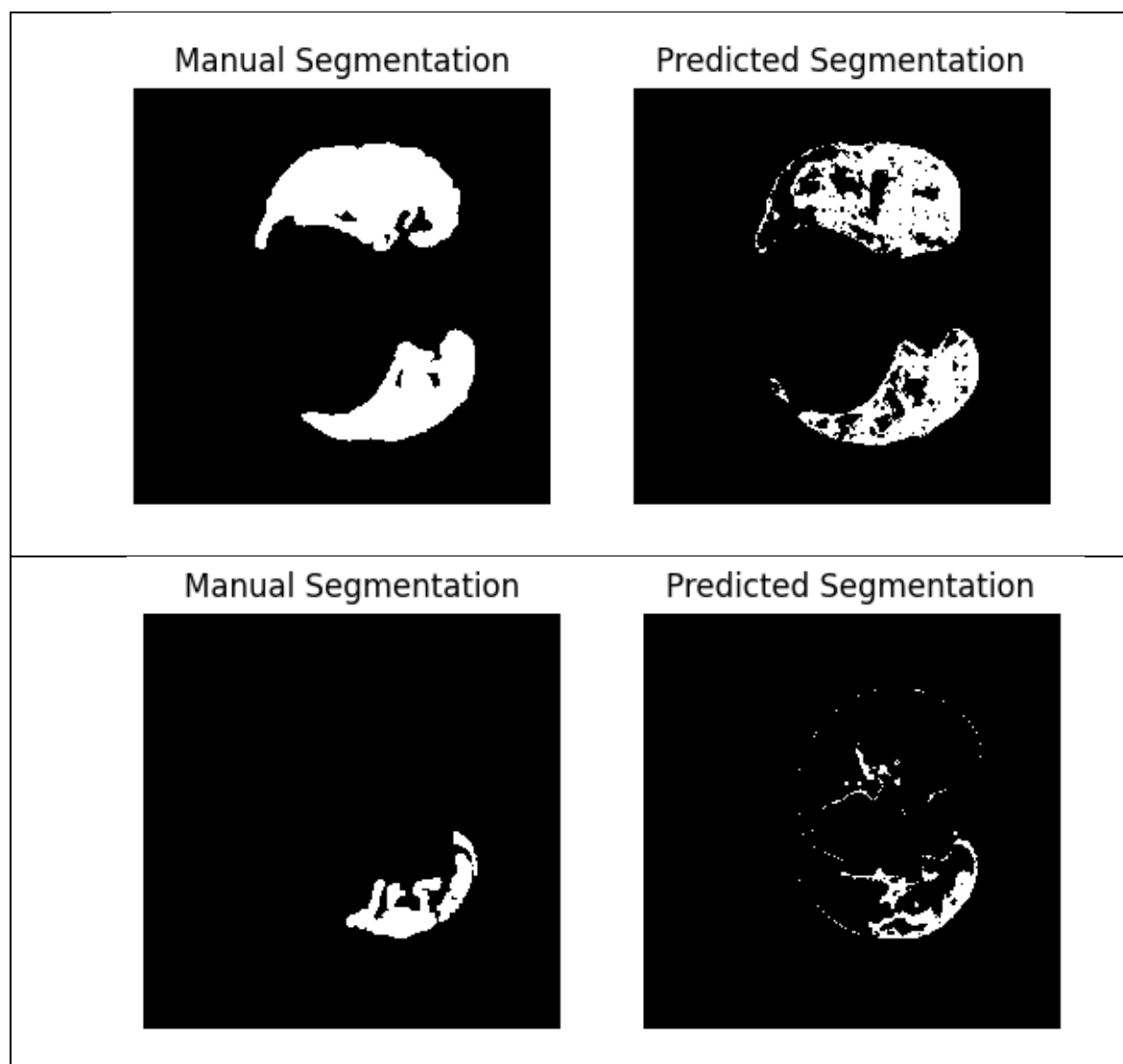


Figure 3: Results of Classification on two selected samples (before and after segmentation)

4 Conclusion

This paper suggests a method for automatic segmentation in chest CT images. In this work, the proposed method is able to extract features and segment automatically the infected regions from the lung image areas. The proposed methodology obtained promising results with an average accuracy, sensitivity and precision of 79.94%, 88.37% and 85.12% values, respectively. This work is useful in the development of methods to detect chest abnormalities based on image analysis and pattern classification in order to provide better diagnoses to the patients using low cost technologies.

As a future work we are currently exploring new features and methods such as deep learning for accomplishing better classification rates and more accurate diagnosis.

References:

- [1] Coronavirus update (Live): 31,170,134 Cases and 964,065 Deaths from COVID-19 Virus Pandemic -Worldmeter n.d. <https://www.worldometers.info/coronavirus/>
- [2] Corman VM, Landt O, Kaiser M, Molenkamp R, Meijer A, Chu DK, et al. Detection of 2019 novel coronavirus (2019-nCoV) by real-time RT-PCR. *Eurosurveillance* 2020;25:2000045.
- [3] Ai T, Yang Z, Hou H, Zhan C, Chen C, Lv W, et al. Correlation of chest CT and RT-PCR testing in coronavirus disease 2019 (COVID-19) in China: a report of 1014 cases. *Radiology* 2020, <http://dx.doi.org/10.1148/radiol.2020200642>.
- [4] Hu Q, Guan H, Sun Z, Huang L, Chen C, Ai T, Pan Y, Xia L, Early CT features and temporal lung changes in COVID-19 pneumonia in Wuhan, China, *European Journal of Radiology* (2020), doi: <https://doi.org/10.1016/j.ejrad.2020.109017>
- [5] Huang C, Wang Y, Li X, et al. Clinical features of patients infected with 2019 novel coronavirus in Wuhan, China. *Lancet*. 395(10223) (2020) o 497-506. doi: 10.1016/S0140-6736(20)30183-5.
- [6] J Kanne JP. Chest CT findings in 2019 novel coronavirus (2019-nCoV) infections from Wuhan, China: key points for the radiologist. Feb 4(2020)200241.
- [7] Shi, Heshui & Han, Xiaoyu & Jiang, Nanchuan & Cao, Yukun & Alwalid, Osamah & Gu, Jin & Fan, Yanqing & Zheng, Chuansheng. (2020). Radiological findings from 81 patients with COVID-19 pneumonia in Wuhan, China: a descriptive study. *The Lancet Infectious Diseases*. 20. 10.1016/S1473-3099(20)30086-4.
- [8] COVID-19 CT segmentation dataset: <http://medicalsegmentation.com/COVID19/>
- [9] Johannes Hofmanninger, Forian Prayer, Jeanny Pan, Sebastian Röhrich, Helmut Prosch and Georg Langs. "Automatic lung segmentation in routine imaging is a data diversity problem, not a methodology problem". 1 2020.
- [10] A. Ravishankar, S. Anusha, H. K. Akshatha, A. Raj, S. Jahnavi and J. Madhura, "A survey on noise reduction techniques in medical images," *2017 International conference of Electronics, Communication and Aerospace Technology (ICECA)*, Coimbatore, 2017, pp. 385-389, doi: 10.1109/ICECA.2017.8203711.
- [11] Senthil Kumar, K et al. "Lung Cancer Detection Using Image Segmentation by means of Various Evolutionary Algorithms." *Computational and mathematical methods in medicine* vol. 2019 4909846. 8 Jan. 2019, doi:10.1155/2019/4909846
- [12] Manoj Diwakar, Manoj Kumar, A review on CT image noise and its denoising, *Biomedical Signal Processing and Control*, Volume 42, 2018, Pages 73-88, ISSN 1746-8094.
- [13] Y. Zimmer, S. Akselrod, R. Tepper, The distribution of the local entropy in ultrasound images, *Ultrasound Med. Biol.* 22 (1996) 431–439.
- [14] J. Barba, H. Jeanty, P. Fenster, J. Gil, The use of local entropy measures in edge detection for cytological image analysis, *J. Microsc.* 156 (1989) 125–134.
- [15] Jing-jing Zong, Tian-shuang Qiu, Wei-dong Li, Dong-mei Guo, Automatic ultrasound image segmentation based on local entropy and active contour model, *Computers & Mathematics with Applications*, Volume 78, Issue 3, 2019, Pages 929-943, ISSN 0898-1221, <https://doi.org/10.1016/j.camwa.2019.03.022>.
- [16] Dalal, N and Triggs, B, Histograms of Oriented Gradients for Human Detection, *IEEE Computer Society Conference on Computer Vision and Pattern Recognition 2005 San Diego, CA, USA*

- [17] Saygılı A, Albayrak S. A new computer-based approach for fully automated segmentation of knee meniscus from magnetic resonance images. *Biocybern Biomed Eng* 2017;37(3):432–42.
- [18] Weiwei Wang, Cuiling Wu, Image segmentation by correlation adaptive weighted regression, *Neurocomputing*, Volume 267, 2017, Pages 426-435, ISSN 0925-2312, <https://doi.org/10.1016/j.neucom.2017.06.046>.
- [19] B. Li, K. Cheng, Z. Yu, Histogram of oriented gradient based GIST feature for building recognition, *Computational intelligence and neuroscience*, 2016 (2016) 10.
- [20] R. Prates, G. Cámara-Chávez, W.R. Schwartz, D. Menotti, Brazilian license plate detection using histogram of oriented gradients and sliding windows, *arXiv preprint arXiv:1401.1990*, (2014).
- [21] X. Zhang, F. An, I. Nakashima, A. Luo, L. Chen, I. Ishii, H.J. Mattausch, A hardware-oriented histogram of oriented gradients algorithm and its VLSI implementation, *Japanese Journal of Applied Physics*, 56 (2017) 04CF01.
- [22] Danny Petschke, Torsten E.M. Staab, A supervised machine learning approach using Naive Gaussian Bayes classification for shape-sensitive detector pulse discrimination in positron annihilation lifetime spectroscopy (PALS), *Nuclear Instruments and Methods in Physics Research Section A: Accelerators, Spectrometers, Detectors and Associated Equipment*, Volume 947, 2019, 162742, ISSN 0168-9002,
- [23] Marina Sokolova, Guy Lapalme, A systematic analysis of performance measures for classification tasks, *Information Processing & Management*, Volume 45, Issue 4, 2009, Pages 427-437, ISSN 0306-4573.